

Elastic scattering of acoustic phonons in Si

J. A. Shields

Department of Physics and Materials Research Laboratory, University of Illinois at Urbana-Champaign, Urbana, Illinois 61801

S. Tamura

Department of Engineering Science, Faculty of Engineering, Hokkaido University, Sapporo, Japan

J. P. Wolfe

Department of Physics and Materials Research Laboratory, University of Illinois at Urbana-Champaign, Urbana, Illinois 61801

(Received 2 August 1990)

We have measured the elastic-scattering rate of high-frequency acoustic phonons in Si by combining the phonon-imaging technique, a unique sample geometry, and Monte Carlo calculations that incorporate the full elastic anisotropy of the crystal. A slotted crystal allows us to separate the purely scattered component of a heat pulse from the combined scattered and ballistic components. A series of Monte Carlo simulations is performed to predict the ratio of scattered to ballistic phonons for varying scattering strengths. Thus the experimentally measured fraction of scattered phonons can be compared with these simulations to yield a scattering rate. This procedure is necessary in order to take into account (1) the distribution of phonon frequencies, (2) the huge anisotropies in heat flux associated with phonon focusing, and (3) lifetime of the phonon source. For a high-purity Si crystal, the measured rate is found to be within experimental uncertainties of that predicted for mass-defect scattering from naturally occurring isotopes.

I. INTRODUCTION

Historically, the most important method for characterizing the scattering of phonons in solids has been thermal conductivity. A temperature dependence of the conductivity yields the frequency dependence of the scattering rate because the mean frequency of a Planckian distribution of phonons increases linearly with the lattice temperature. This "spectroscopic" technique has provided valuable information about scattering from defects in many crystalline and disordered solids.¹

The simplest "mass defects" in a crystal arise from the natural occurrence of atoms with differing isotopic mass. Nevertheless, very few quantitative measurements of isotope scattering have been performed—largely because extrinsic defects can easily dominate this effect. The classic observation of isotope scattering was performed on Ge, employing a special isotopically pure sample for comparison.²

With the advent of heat-pulse techniques, which have the ability to detect ballistic phonons of selected polarization (longitudinal or transverse) and propagation direction, one might hope to make systematic measurements of impurity and isotope scattering. Specifically, it should be possible to separate the ballistic and scattered components of a heat pulse by their differing times of flight across the crystal. Indeed, nearly all heat-pulse experiments performed at liquid-helium temperatures show a sharp pulse at the ballistic transit time and a long "tail" due to phonons which have scattered in the bulk. An example of this experimental situation is the heat-pulse signals in Si shown in Fig. 1, obtained for slightly different propagation directions, as described below. The extreme

variations of ballistic flux with propagation direction imply that a simple ratio of scattered to ballistic signals (appropriately integrated), does not directly yield the scattering rate.

Actually, there are several difficulties in determining the scattering rate from this time-of-flight information: (1) determining the phonon frequencies, (2) accounting

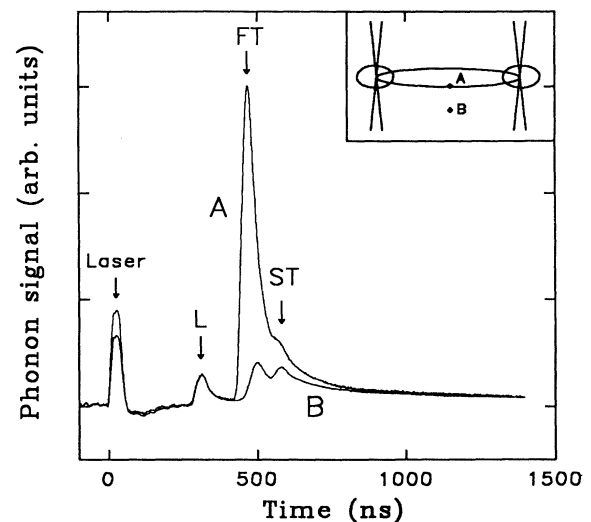


FIG. 1. Detected phonon intensity vs time for a point on the FT caustic (upper curve) and just off the FT caustic (lower curve) showing the large change in the ballistic signal intensity for a small change in propagation direction ($\Delta\theta \approx 5^\circ$). The positions of the two points are indicated in the inset.

for spatial anisotropies (i.e., phonon focusing), and (3) knowing the lifetime of the phonon source (i.e., hot-spot effects). We now briefly discuss each of these effects and their remedies.

Phonon frequency is the essence of the problem. Scattering of phonons from mass defects is an example of Rayleigh scattering, which is given by the well-known formula³

$$\tau^{-1} = A_0 v^4, \quad (1)$$

$$A_0 \approx ca^3 \left[\frac{\Delta m}{m} \right]^2 \frac{(2\pi)^4}{4\pi v^3},$$

where τ is the scattering time, v is the phonon frequency, a is the lattice constant, v is the sound velocity, m is the mass of the host atom, Δm is the difference in host and defect masses, and c is the concentration of defect masses. This formula assumes a simple monatomic lattice with one type of defect. The key point is that the frequency dependence is extremely rapid, so an experiment aiming to determine the scattering rate must determine frequency very carefully. The nature of a heat-pulse experiment implies that a distribution of frequencies is present, so this means that some modeling is required in the analysis. (Thermal conductivity, which involves the equilibrium Planck distribution of phonons, also suffers from this fate.) As we shall see, the frequencies in a heat-pulse experiment can be greatly restricted by appropriate selection of a phonon detector.

The second difficulty involves elastic anisotropy. It is well known that a point source of heat emits phonons in a highly anisotropic distribution—an effect known as phonon focusing.⁴ This greatly impacts the measurement of the scattering rate because the intensity of the ballistic signal depends sensitively on the direction chosen between the heat source and detector, and even on the sizes and shapes of the source and detector. That is, the ballistic-to-scattered ratio depends critically on the ballistic propagation direction. To illustrate this effect, Fig. 1 shows the large change in the ballistic signal of fast transverse (FT) phonons when the propagation direction is changed only a small amount—on and off a phonon caustic.

Immediately one might wonder if the *scattered* phonon flux exhibits any anisotropy. Previous work by Ramsbey *et al.*⁵ and by Shields *et al.*⁶ has shown that phonons scattered just a few times retain some of the anisotropy exhibited by the ballistic phonons. This so-called “channeling” effect must be properly accounted for in a measurement of the scattering rate.

The third major difficulty is determining whether the tail of the heat pulse is due to scattering in the bulk or to a finite lifetime of the phonon source. It is known that at high excitation levels, whether from Ohmic heating or laser excitation, a heated region of diffusive phonon propagation (a “hot spot”) may be formed which can have a lifetime longer than the excitation pulse.^{7–10} Also, direct photoexcitation of a semiconductor can produce excited electronic states (e.g., excitons and electron-hole droplets) with significant lifetimes.

In view of these hurdles, it is little wonder that quanti-

tative measurements of scattering rates are rarely attempted using the heat-pulse technique. Notable exceptions are the recent works of Held *et al.*¹¹ and Fieseler *et al.*,¹² who employ the phonon-imaging^{13,14} technique to study the scattering of phonons in GaAs.

In this paper we present some key refinements of the heat-pulse method which resolve the aforementioned problems. (1) Frequency selection is imposed by using a superconducting tunnel-junction detector, and the response of this detector is incorporated into the theoretical modeling. (2) Precise control of the phonon propagation direction is achieved by fabricating a tiny detector and using a focused laser beam as an accurately positioned excitation source. Raster scanning the laser beam—i.e., phonon imaging—permits a selection of appropriate phonon-focusing structures. The theoretical modeling contains the full anisotropy of the crystal. (3) To avoid effects of source lifetime, we employ a special sample geometry⁶ to spatially isolate the scattered component of the heat-pulse signal, rather than relying on the exact temporal shapes of the heat pulses.

The present measurements are the first, we believe, to measure the elastic scattering rate in an ultrapure crystal of silicon. The measured rate is very close indeed to the isotope scattering rate predicted for this crystal. These experiments also forecast a basic method for quantitative measurements of phonon scattering from extrinsic defects.

II. THE EXPERIMENT

A schematic diagram of the basic experiment is shown in Fig. 2(a). A phonon detector is centered on one face of a silicon crystal,¹⁵ which is immersed in liquid helium at $T = 1.7$ K. A 2000-Å copper film is deposited on the opposite face, which is locally heated by a focused laser beam. Both surfaces are polished with 1 μm diamond paste followed by a Syton[®] polish. As in the standard phonon-imaging experiment of Northrop and Wolfe,¹³ the laser beam may be fixed, or scanned across the face of the crystal.

The silicon crystal is slotted about halfway through with a “gentle” string-saw cut.⁶ When the laser spot is behind the slot, as viewed from the detector, the ballistic flux is completely blocked, as indicated in Fig. 2(b). For this laser-spot position only scattered phonons are detected. With a slight displacement to the right, both scattered and ballistic components become observable, as schematically shown in Fig. 2(c). With this information it is possible to directly determine a ratio of ballistic-to-scattered phonon flux.

Before describing the results, we mention a few pertinent details in the experiment. The laser is a cavity-dumped Ar⁺ ($\lambda \sim 5000$ Å) with a pulse width of 10 ns and a typical incident pulse energy of 10–50 nJ. The beam is focused to a spot about 10 μm in diameter and raster scanned by means of galvanometer-mounted mirrors under computer control. The detector is a PbBi superconducting tunnel junction with $10 \times 10 \mu\text{m}^2$ sensitive area, as described by Hebboul and Wolfe.¹⁶ The superconducting gap can be adjusted by varying the ratio of Bi to

Pb. Most of the data are taken with a measured superconducting gap of $2\Delta = 2.8 \pm 0.1$ meV, which implies that only phonons with a frequency above $2\Delta/h = 680 \pm 25$ GHz are detected. A boxcar integrator selects the time interval over which the phonon signals are recorded, which in these experiments is usually set to be between t_b and $1.5t_b$, where t_b is the ballistic time for the phonon mode being considered. The boxcar output, which is proportional to the heat flux for a given laser-spot position, is stored in a computer.

The crystal is cut with (110) faces for the detector and excitation surfaces, making the depth of the slot not critical, since the phonon intensity is smoothly varying perpendicular to the slot boundary. A wide-angle phonon-focusing pattern for an unslotted silicon crystal is shown in Fig. 3(a). The bright areas indicate regions of high phonon flux.¹⁷ For the sample dimensions shown in Fig. 2(a), only a small section at the center of this pattern is observable, and the slot allows only observation of the right half of the ballistic pattern. Figure 3(b) shows an experimental image for the slotted crystal. The ballistic signals on the right side of the image show the fast transverse (FT) ridge bounded by two caustics. The left side of the image (behind the slot) shows the much weaker scat-

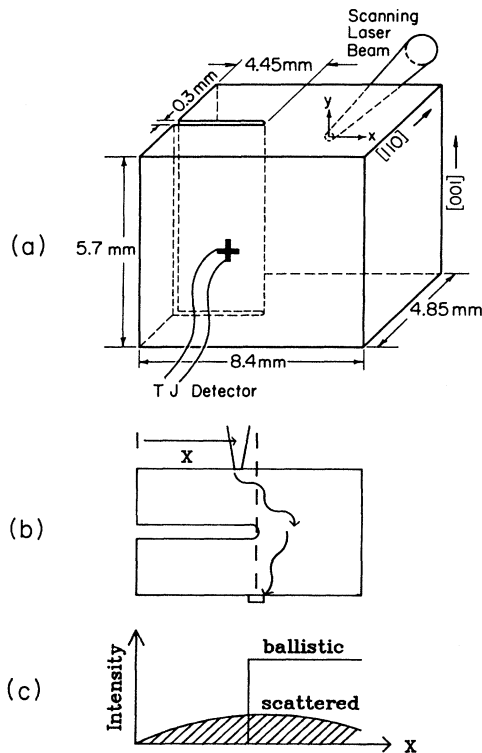


FIG. 2. (a) Schematic of the "slotted" sample geometry. The slot in the crystal is positioned approximately halfway between two (110) faces and extends approximately halfway into the crystal. The detector is deposited on the front face while the laser is raster scanned across the back face. (b) Top view of the sample geometry showing the path of a once-scattered phonon. (c) Schematic of the expected intensity distribution for this sample geometry.

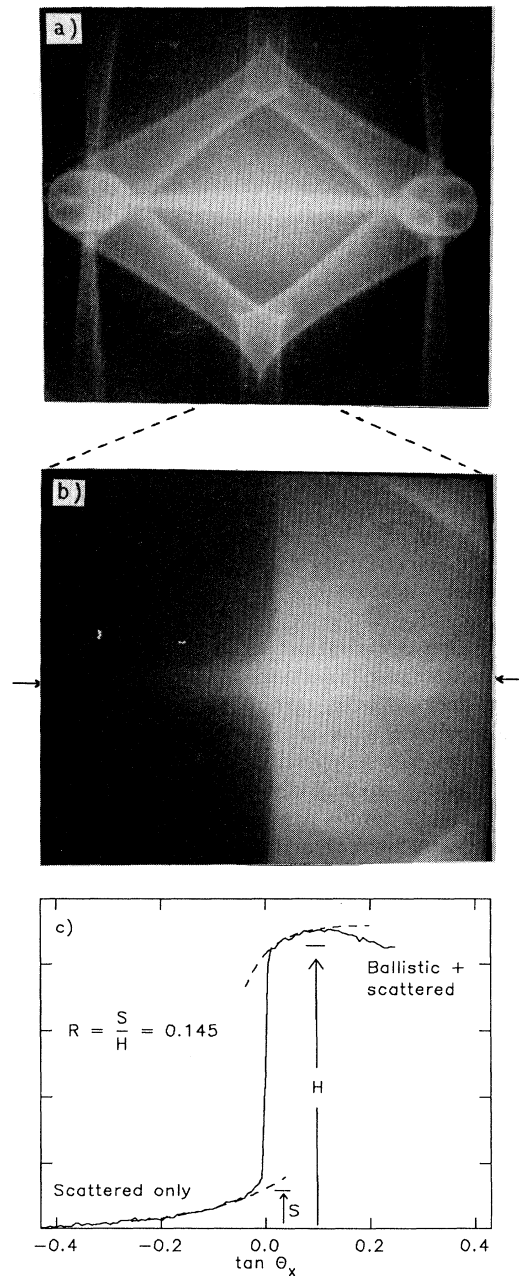


FIG. 3. (a) Experimental phonon image of a $9.4 \times 5.6 \times 2.5$ mm³ unslotted Si crystal with (110) excitation and detection surfaces, showing the phonon-focusing pattern obtained with a detector with an onset frequency of 820 GHz. (b) Experimental phonon image of the slotted sample shown in Fig. 2(a). The slot boundary is along a vertical line through the center of the image and the scattered phonons can be seen weakly on the left side of the image. The image was taken using a tunnel-junction detector with a 680-GHz onset frequency. The intensity of the phonons on the left side of the image has been photographically enhanced to accentuate the scattered phonons. (c) Phonon intensity vs angle for the line marked in image (b). The ledge ratio R is the ratio of the scattered to total phonon intensities at the slot.

tered flux. A weak continuation of the FT ridge behind the slot is the “channeling effect” described in Refs. 5 and 6.

To get a quantitative measure of the phonon scattering in this crystal, we examine a single horizontal line across the image—through the center of the FT ridge. (Actually, the vertical scan is turned off, and a horizontal line scan is slowly recorded.) The result shown in Fig. 3(c) may be compared to the schematic drawing in Fig. 2(c). A more complete picture of the heat flux may be displayed as a pseudo-three-dimensional (3D) representation of the image, as in Fig. 4. For quantitative information, however, we concentrate on the single line scan in the (100) plane, Fig. 3(c).

From this data, we define a “ledge ratio” $R = S/H$, which indicates the fraction of scattered flux, as shown in Fig. 3(c). Ideally, for two laser-spot positions displaced infinitesimally to the left and the right of the slot boundary, the scattered flux should be nearly the same. However, since the slot does not produce an infinitely sharp cutoff (due to the finite source size and subsurface crystal damage in the slot proximity), we extrapolate the signals on either side of the slot, as shown, fitting the data to exponential functions. A vertical line is drawn through the midpoint of the ledge dropoff, and the intersection of this line with the fitted curves determines S and H .

We find that the ledge ratio is relatively insensitive to adjustable experimental parameters such as power level, gate width, and surface preparation. Figure 5(a) shows the dependence of the ledge ratio on excitation power for two experiments employing detectors with different onset frequencies as indicated in the figure. As expected, the experiment with the 850-GHz onset frequency shows a larger ledge ratio (stronger scattering) than that with the 680-GHz onset frequency. For an order of magnitude change in power, R changes only about 25%. This suggests that the frequency distribution of the detected phonons is not changing significantly over this range of excitation powers. We shall see from a Monte Carlo calculation

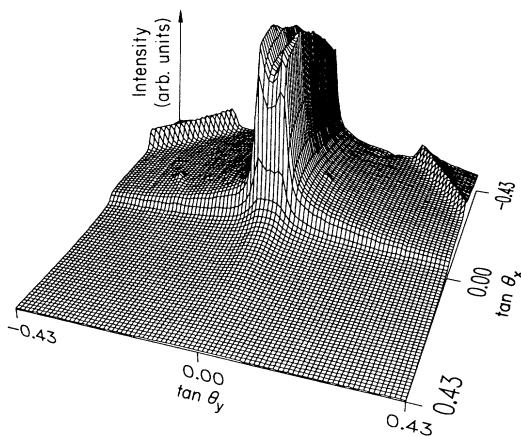


FIG. 4. Pseudo-3D representation of the experimental image shown in Fig. 3(b). This view is from the left side of the image looking toward the slot boundary; x and y scan directions are shown in Fig. 2. The scattered signal is in the foreground and the ballistic features are in the background.

described in the next section that the detected frequencies fall in a narrow region above the onset frequency of the detector.

As shown in Fig. 5(b), the ledge ratio does depend on the chosen gate width. For a narrow sampling window centered around the ballistic time of flight t_b , the scattered flux is largely excluded. However, for sampling gates beginning just before the ballistic onset time t_b and having widths between about $0.2t_b$ and $0.6t_b$ the ledge ratio is nearly constant. At gate widths larger than $1.6t_b$, the ledge ratio is observed to rise slowly. This increase may be partly due to phonons which have scattered off

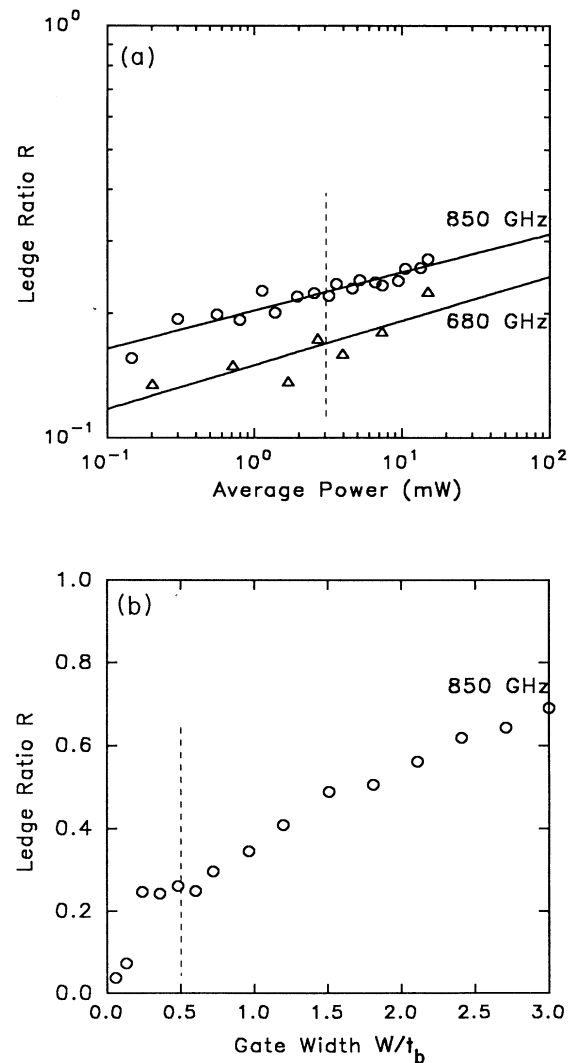


FIG. 5. (a) Power dependence of the ledge ratio. The data of Fig. 3(c) were taken at a power of 3 mW as indicated by the vertical dashed line. Data for both 680- and 850-GHz tunnel-junction detectors are shown. (b) Gate-width dependence of the ledge ratio. The vertical dashed line indicates the value used for the data of Fig. 3(c). The rise in R for a gate width larger than $0.6t_b$ probably corresponds to the detection of phonons scattered from the sidewalls. These data were taken using an 850-GHz tunnel-junction detector.

the side surfaces of the crystal. By choosing a gate width of $0.5t_b$, we therefore exclude this sidewall scattering. For this restricted sampling time, and for these rather small values of R , the scattered signal S is primarily due to singly scattered phonons.

Therefore, by choosing a restrictive time window for observation, we are minimizing effects due to surface scattering, which depend on sample geometry and boundary conditions. Scattering at a surface may be specular or diffuse,^{18,19} depending on the surface preparation, and the transmission of the phonons depends on the adjoining medium (e.g., metal film, liquid helium, vacuum). In our experiment, scattering from the excitation or detection surface would involve at least three straight phonon paths before reaching the detector, with one of them in the detector-to-source direction, implying that the surface scattered phonons will contribute to the detected flux mainly at times later than our chosen time gate.

III. THEORY OF ELASTIC SCATTERING IN AN ANISOTROPIC MEDIUM

Although the simple formula (1) for the mass-defect scattering describes the essential feature of the phonon scattering by isotopic atoms, some modifications are needed to apply it to the quantitative studies of elastic scattering of phonons in silicon. In addition, for a Monte Carlo simulation of the scattering, we also need a formula describing the probability of scattering for particular phonon modes and wave vectors. So, here we briefly recapitulate the derivation of the isotope scattering rate of long-wavelength acoustic phonons in an anisotropic medium.

According to the lowest-order perturbation theory, the scattering rate Γ ($=\tau^{-1}$) of phonons by randomly distributed isotopic atoms is given by^{20,21}

$$\Gamma_\lambda = \frac{\pi}{2N} g \omega_\lambda^2 \sum_{\lambda'} \delta(\omega_\lambda - \omega_{\lambda'}) |\mathbf{e}_\lambda \cdot \mathbf{e}_{\lambda'}|^2, \quad (2)$$

where $\lambda = (\mathbf{k}, j)$ specifies the wave vector \mathbf{k} and mode j of a phonon, N is the number of atoms, g is a factor measuring the magnitude of mass fluctuations caused by isotopic atoms, $\omega = 2\pi\nu$ is the angular frequency, and \mathbf{e} is the polarization vector. More explicitly, the factor g is defined by

$$g = \sum_i f_i \left[1 - \frac{m_i}{\bar{m}} \right]^2, \quad (3)$$

where f_i is the fraction of i th isotope with mass m_i and $\bar{m} = \sum_i f_i m_i$ is the mean atomic mass. If we use the following equation, valid for a cubic crystal:

$$\sum_\lambda (e_\lambda)_\alpha (e_\lambda)_\beta F_\lambda = \frac{1}{3} \delta_{\alpha\beta} \sum_\lambda F_\lambda, \quad (4)$$

where F_λ is some general function depending on λ , we can eliminate the polarization vectors from Eq. (2) and obtain

$$\Gamma_\lambda = \frac{\pi}{6} V_0 g \omega_\lambda^2 D(\omega_\lambda), \quad (5)$$

where V_0 is the volume per atom and the phonon density of states D per unit volume is given by

$$D(\omega) = \frac{\omega^2}{(2\pi)^3} \sum_j \int_\omega \frac{d\Omega_\lambda}{v_\lambda^3}, \quad (6)$$

where the integral is taken over the solid angle Ω_λ subtended by the constant-frequency ($\omega_\lambda = \omega$) surface of the phonon λ in wave-vector space and v_λ is the phase velocity. Hence, by putting

$$\frac{1}{\langle v^3 \rangle} = \frac{1}{3} \sum_j \int_\omega \frac{d\Omega_\lambda}{4\pi} \frac{1}{v_\lambda^3} \quad (7)$$

we find

$$\Gamma_\lambda = \frac{V_0}{4\pi} g \frac{\omega_\lambda^4}{\langle v^3 \rangle} = A_0 v_\lambda^4. \quad (8)$$

This is the necessary refinement of Eq. (1). Equation (8) depends on λ only through the frequency ω_λ and hence the total isotope scattering rates is independent of the mode and propagation direction of the initial phonon. Numerically, we obtain the result $A_0 = 2.43 \times 10^{-42} \text{ sec}^3$ for silicon.

For the Monte Carlo simulation, we have to keep track of each phonon, possibly scattering several times before reaching the detector. For this purpose, we also need to know the probability for a phonon to be mode converted and scattered in a specified direction in wave-vector space. This probability $\gamma_{\lambda\lambda'}$ for the scattering from phonon λ to phonon λ' is derived from Eq. (2) by rewriting it as

$$\Gamma_\lambda = \sum_{\lambda'} \int_{\omega_\lambda} \frac{d\Omega_{\lambda'}}{4\pi} \gamma_{\lambda\lambda'}. \quad (9)$$

Thus we get the polarization-vector-dependent result

$$\gamma_{\lambda\lambda'} = \frac{V_0}{4\pi} g \omega_\lambda^4 \frac{|\mathbf{e}_\lambda \cdot \mathbf{e}_{\lambda'}|^2}{v_{\lambda'}^3}. \quad (10)$$

This equation indicates that the scattering is quite anisotropic, i.e., the intramode scattering occurs predominantly in the forward and backward directions but the intermode scattering mainly perpendicular to the initial propagation direction. We also find that the scattering into TA phonons dominates the scattering into LA phonons due to the presence of the factor of $v_{\lambda'}^{-3}$. More precisely, the relative magnitudes of the scattering into the three acoustic branches in silicon are 0.531, 0.376, and 0.093 for the scatterings into slow transverse (ST), FT, and LA branches, respectively. Here we note that the polarization-vector dependence of the individual scattering events, as shown in Eq. (10), is the origin of the channeling of elastically scattered phonons observed recently by phonon-imaging experiments.^{5,6} The isotropic approximation for the scattering, i.e., the elimination from Eq. (10) of the polarization-vector dependence in the scattering rate by setting $|\mathbf{e}_\lambda \cdot \mathbf{e}_{\lambda'}|^2 = \frac{1}{3}$, has been shown to be inconsistent with the strong channeling in the experimental data.

The Monte Carlo simulation of phonon propagation in the slotted geometry is performed with procedures simi-

lar to those described in Refs. 5 and 6. A large number of starting phonons are assumed to be excited at a surface point of the (110)-oriented silicon sample. Each phonon is assigned a frequency higher than the onset frequency of the detector weighted by the Planck distribution²² with an appropriate value of heater temperature (e.g., 10 K). As will be shown later, the Monte Carlo result is rather insensitive to the values of the heater temperature. The phonons are emitted randomly into the crystal with an isotropic distribution in wave-vector space. The relative population of the initial phonons of each mode is specified to be proportional to the density of states ($\sim v_\lambda^{-3}$). Γ_λ is used to generate the time for the first scattering event and the initial group velocity is used to find the position at which the scattering event occurs for each phonon. The surface position and arrival times are recorded for phonons crossing the detection surface of the crystal. Phonons crossing the slot or those traveling longer than an assumed time of flight ($1.5t_b$, with t_b as the ballistic time of flight for FT phonons traveling the sample thickness along the [110] direction) before hitting the surface are discarded. If scattering occurs inside the crystal, we use $\gamma_{\lambda\lambda'}$ to calculate the mode and propagation direction of the scattered phonon and the process is repeated. We assume that the sample is infinitely extended parallel to the surfaces; i.e., no scattering at the sidewalls is assumed. If a phonon crosses the excited crystal surface it is also discarded by assuming that liquid

He is a highly absorbing medium of phonons. In this manner we have counted 3×10^5 phonons hitting the rectangular area limited by $|\tan\Theta_x| \leq 0.6$ and $|\tan\Theta_y| \leq 0.3$ (Θ_x and Θ_y are measured from the [110] direction) on the detector surface of the sample within the assumed time gate. For each phonon we have recorded the x and y coordinates, arrival time, frequency, and number of scattering events.

The two-dimensional distribution of the phonons on the detector surface is shown in Fig. 6(a). In this figure, the density of dots is proportional to the phonon intensity. In Fig. 6(b) the corresponding pseudo-3D representation for the phonon intensity distribution is plotted. A continuation of the FT ridge behind the slot is clearly evident. This is due to the channeling effect of the scattered FT phonons, as previously observed for (100)-oriented silicon.⁶ Comparison to the experimental image in Fig. 4 shows that the FT ridge is wider than the calculation. This indicates that the dispersive shift of the FT phonon caustics is significant even for phonons with a frequency of 0.7 THz in silicon. A detailed discussion on the dispersive shifts and the effect of dispersion on the isotope scattering in silicon is planned for a separate paper.

As stated above, the Monte Carlo results are rather insensitive to the chosen value of the heater temperature. Line traces across the slot boundary for two different values of the heater temperature (10 and 30 K) are shown in Fig. 7. As can be seen from the figure, the ledge ratio is virtually identical for the two traces, despite the large temperature difference. This similarity can be explained by examining the frequency distribution of the detected phonons as shown in Fig. 8. Both total and scattered flux are shown for each temperature. The corresponding curves for 10 and 30 K are remarkably similar considering that the peak of the Planck distribution scales linearly

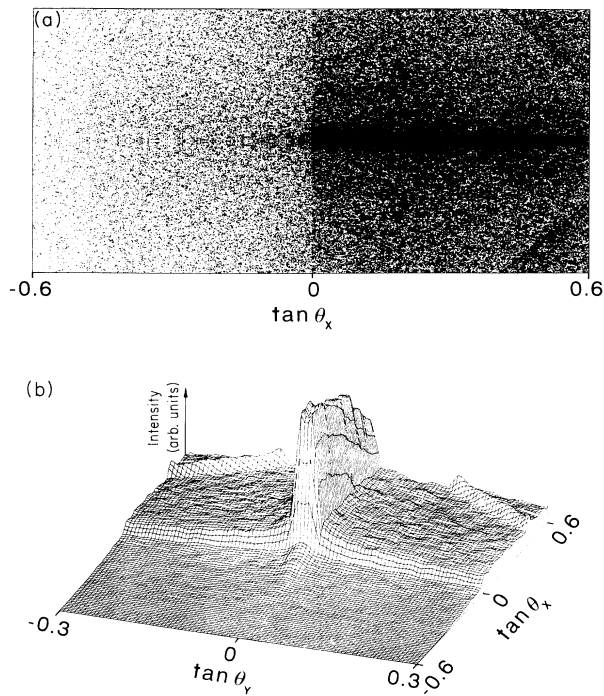


FIG. 6. Monte Carlo calculations assuming elastic scattering at the theoretical isotope scattering rate and the slotted sample geometry shown in Fig. 2(a). (a) Calculated phonon flux with the slot at the center. (b) Pseudo-3D representation of the image in (a).

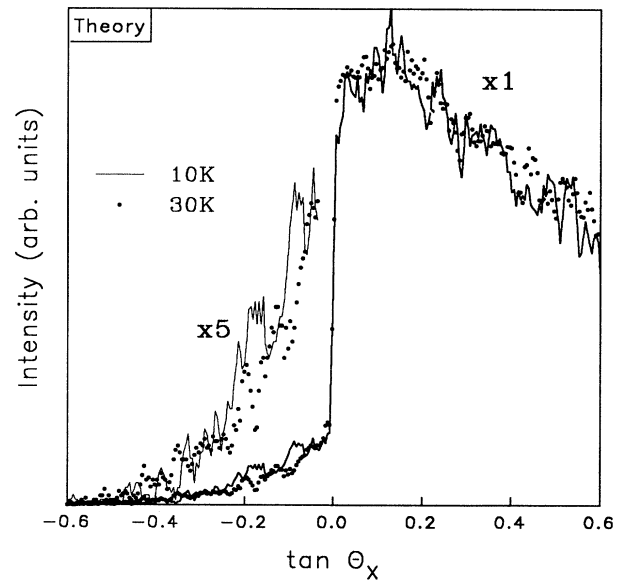


FIG. 7. Theoretical line scans for temperatures of 10 and 30 K, showing the insensitivity of the ledge ratio to source temperature.

with temperature. Also, remember that the ledge ratio is determined by the *ratio* of scattered to total phonons. The high-frequency phonons are selected against by both the signal time gate and the increased scattering rate of the higher-frequency phonons. This is because the higher-frequency phonons have slower velocities (due to dispersion) and scatter more often, both leading to longer travel times from source to detector. The $0.5t_b$ time gate diminishes the signal due to these higher-frequency phonons.

IV. DETERMINATION OF THE SCATTERING RATE

A brute force approach to determining the scattering rate in our sample of silicon would be to adjust the scattering rate in the Monte Carlo simulations until there is a good overall agreement with the experimental image. This is not practical, at least at the present time, because exact registration of the experimental and theoretical focusing patterns would be required, and least-squares fitting would imply many iterations of the time-intensive Monte Carlo simulations. Indeed, an entire array of 64 000 data points is hardly necessary to determine a single characteristic scattering time τ . The next simplest approach would be to compare theoretical and experimental line scans in the (100) plane, as we have plotted in Figs. 3(c) and 7. Still, this requires significant fitting time. Our present approach is to make use of the (100) line scan, but, as previously discussed in Fig. 3, to reduce this information to a single representative number—the ledge ratio, $R = S/H$. (Our determination of R , however, does make use of most of the data along the line scan.) We have seen that for a given geometry and time selection, this parameter is principally determined by the bulk scattering time τ .

Figure 9(a) shows a separation of the calculated flux into its ballistic and scattered components, assuming

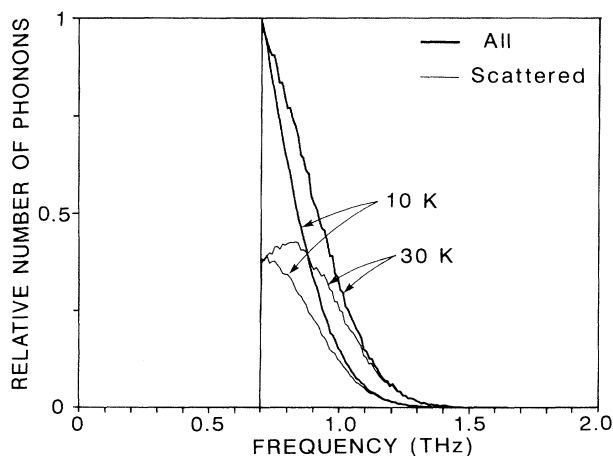


FIG. 8. Frequency distribution of detected phonons for two different source temperatures (for the same time gate of $0.5t_b$) in the Monte Carlo calculation. Both total (upper thick lines) and scattered (lower thin lines) distributions are shown for both 10 and 30 K.

$\tau^{-1} = Av^4$ with $A = A_0$ and a source temperature $T = 10$ K. By symmetry, the ballistic component must reach a maximum at the slot, i.e., along the [110] direction. To accurately determine the peak ballistic signal, we fit the “data” to a fourth-order polynomial, shown as the dashed line on the top. The scattered flux on the left of the slot is fit to a simple exponential, as done for the data in Fig. 3(c). The ledge ratio is thus determined as shown in Fig. 9(b).

This procedure is repeated for six different Monte Carlo calculations, with values of A ranging from $0.1A_0$ to $2.0A_0$. The solid circles in Fig. 10 show the results of these calculations. Between $0.25A_0$ and $2.0A_0$, the ledge ratios determined in this way fit a straight line.

The experimentally determined ledge ratio of $R = 0.145$ [see Fig. 3(c)] is plotted as a horizontal line on this graph. The shaded area gives the statistical uncertainty. The intersection of the horizontal line with the

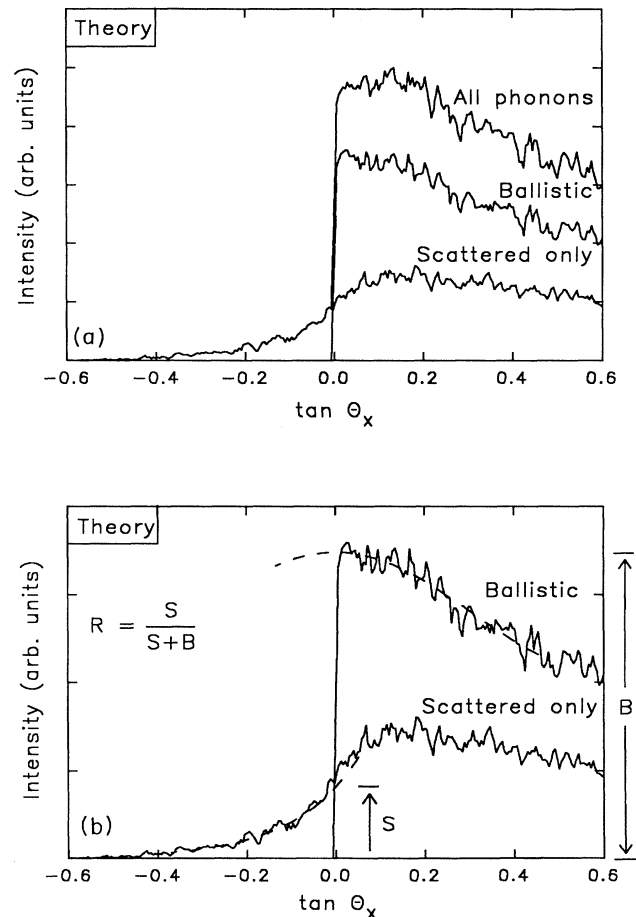


FIG. 9. (a) Separation of the components of the theoretical phonon flux into ballistic and scattered parts assuming $T = 10$ K and $A = A_0$. (b) The ledge ratio is determined for the theoretical line scans by fitting the ballistic part to a fourth-order polynomial (upper dashed curve) and the scattered part at negative angle to an exponential. The ledge ratio is found by computing the value of these functions at the slot position.

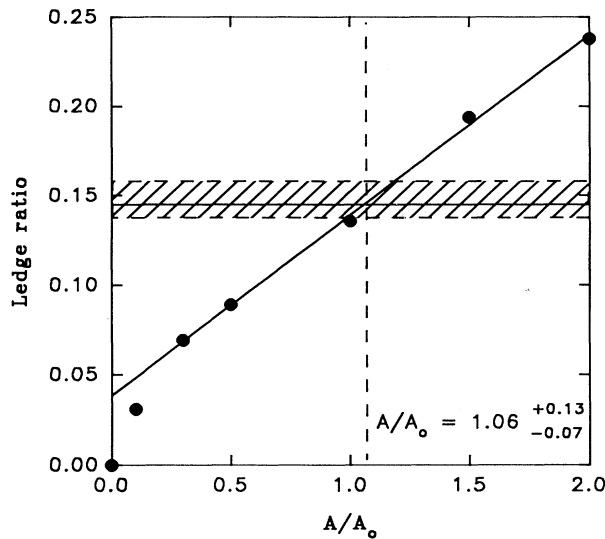


FIG. 10. Determination of the scattering constant. The solid circles are the theoretical values of the ledge ratio assuming various scattering constants. The highest five points are fit to a line. The horizontal line is the experimental value of the ledge ratio. The intersection of the two lines gives the experimentally measured scattering constant.

fitted curve gives the scattering-rate constant appropriate for this silicon crystal. The stated uncertainties, of course, do not include any systematic errors associated with the measurement procedure. From consideration of the adjustable parameters, laser power, and sampling time (Figs. 5 and 7), we feel that the systematic errors should not exceed about 25%. Thus the measured scattering-rate constant for pure silicon is found to be $A = (1.06 \pm 0.3)A_0$. This uncertainty applies to the absolute determination of a scattering rate. For comparison of scattering rates for different crystals under similar conditions, the method we have devised above should have an accuracy of about 10% or better.

The above analysis excludes the longitudinal phonons, which arrive earlier in time than the transverse phonons. While the longitudinal mode should exhibit reduced scattering (due to its larger velocity and thus longer mean free path), the elastic scattering constant A is mode independent and can be recovered from a study of either mode. Defects which change the local symmetry or have low-lying electronic levels, however, may scatter the longitudinal and transverse modes differently and induce new anisotropies into the scattering.

Figure 11 compares experimental and theoretical line scans of the longitudinal signal in the (100) plane, as before. The parameters for the theoretical line scans are identical to those for the transverse calculations except that the time selection is between $t=0$ and $1.5t_b$, where t_b is the ballistic time for the longitudinal mode. As can be seen in the figure, the experimental and theoretical ledge ratios agree quite well when the theoretical calcula-

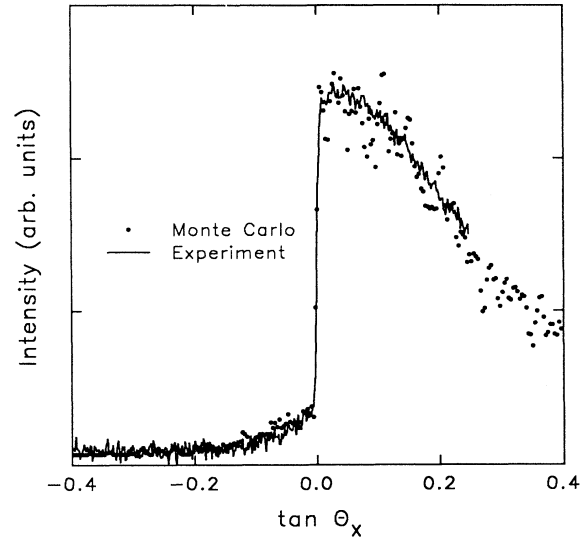


FIG. 11. Experimental data and theoretical Monte Carlo calculations for the longitudinal phonon mode. By assuming a value of the scattering constant to be $A = A_0$, the calculation agrees well with the experimental trace as shown.

tion assumes a value of $A = A_0$ for pure isotope scattering, consistent with the results of the analysis for the transverse phonons above.

V. CONCLUSIONS

In summary, by combining phonon imaging with tunnel-junction detection, a slotted sample geometry, and Monte Carlo calculations, we have performed quantitative measurements of the bulk phonon scattering rates in silicon. The analysis is facilitated by the definition of a dimensionless quantity, the "ledge ratio" associated with the slot, which is directly correlated to the amount of scattering in the sample. Comparison of the measured ledge ratio with that computed by Monte Carlo calculations assuming varying amounts of elastic scattering yields a determination of the scattering rate for our sample. In high-purity silicon the scattering rate determined by this method is nearly identical to that predicted for isotope scattering. Further experiments and calculations including dispersive effects and utilizing detectors with different onset frequencies should provide more direct information about the frequency dependence of the elastic phonon scattering.

ACKNOWLEDGMENTS

This work was supported in part by the National Science Foundation under the Materials Research Laboratory Grant No. DMR-89-20538. The work at Hokkaido University was supported by a Grant-in-Aid for Scientific Research from the Ministry of Education, Science and Culture of Japan (Grant No. 0155001). We thank M. Ramsbey for many useful discussions.

- ¹R. Berman, *Thermal Conduction in Solids* (Clarendon, Oxford, 1976).
- ²T. H. Geballe and G. W. Hull, *Phys. Rev.* **110**, 773 (1958). See also G. A. Slack, *ibid.* **105**, 829 (1957); J. Callaway, *ibid.* **113**, 1046 (1959); V. Ambegaokar, *ibid.* **114**, 488 (1959).
- ³P. G. Klemens, *Proc. Phys. Soc. London, Sect. A* **68**, 1113 (1955).
- ⁴B. Taylor, H. J. Maris, and C. Elbaum, *Phys. Rev. Lett.* **23**, 416 (1969).
- ⁵M. T. Ramsbey, J. P. Wolfe, and S. Tamura, *Z. Phys. B* **73**, 167 (1988).
- ⁶J. A. Shields, J. P. Wolfe, and S. Tamura, *Z. Phys. B* **76**, 295 (1989).
- ⁷J. C. Hensel and R. C. Dynes, *Phys. Rev. Lett.* **39**, 969 (1977).
- ⁸M. Greenstein, M. A. Tamor, and J. P. Wolfe, *Phys. Rev. B* **26**, 5604 (1982).
- ⁹J. A. Shields and J. P. Wolfe, *Z. Phys. B* **75**, 11 (1989).
- ¹⁰*Phonons 89*, edited by S. Hunklinger, W. Ludwig, and G. Weiss (World Scientific, Singapore, 1990), for example, pp. 1225, 1287, and 1290.
- ¹¹E. Held, W. Klein, and R. P. Huebener, *Z. Phys. B* **75**, 17 (1989).
- ¹²M. Fieseler, M. Wenderoth, and R. G. Ulbrich, in *Proceedings of the 19th International Conference on the Physics of Semiconductors*, Warsaw, edited by W. Zawadzki (Polish Academy of Science, Warsaw, 1988).
- ¹³G. A. Northrop and J. P. Wolfe, *Phys. Rev. B* **22**, 6196 (1980).
- ¹⁴G. A. Northrop and J. P. Wolfe, in *Nonequilibrium Phonon Dynamics*, edited by W. E. Bron (Plenum, New York, 1985).
- ¹⁵The high-purity ($N_A - N_D \approx 10^{12} \text{ cm}^{-3}$) crystal was grown by Siemens.
- ¹⁶S. E. Hebboul and J. P. Wolfe, *Z. Phys. B* **73**, 437 (1989).
- ¹⁷D. C. Hurley and J. P. Wolfe, *Phys. Rev. B* **32**, 2568 (1985).
- ¹⁸G. A. Northrop and J. P. Wolfe, *Phys. Rev. Lett.* **52**, 2156 (1984).
- ¹⁹The boundary scattering problem is considered, for example, in D. Marx and W. Eisenmenger, *Z. Phys. B* **48**, 277 (1982) and P. Taborek and D. L. Goodstein, *Phys. Rev. B* **22**, 1550 (1980).
- ²⁰P. Carruthers, *Rev. Mod. Phys.* **33**, 92 (1961).
- ²¹S. Tamura, *Phys. Rev. B* **27**, 858 (1983).
- ²²O. Weis, *Z. Angew. Phys.* **26**, 325 (1969).

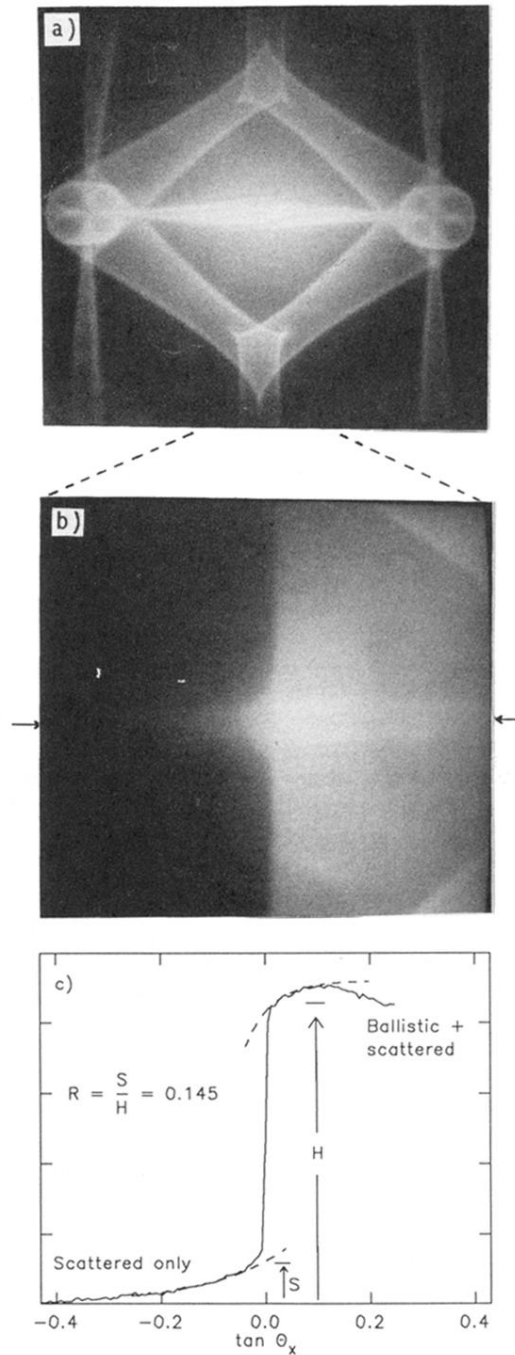


FIG. 3. (a) Experimental phonon image of a $9.4 \times 5.6 \times 2.5$ mm^3 unslotted Si crystal with (110) excitation and detection surfaces, showing the phonon-focusing pattern obtained with a detector with an onset frequency of 820 GHz. (b) Experimental phonon image of the slotted sample shown in Fig. 2(a). The slot boundary is along a vertical line through the center of the image and the scattered phonons can be seen weakly on the left side of the image. The image was taken using a tunnel-junction detector with a 680-GHz onset frequency. The intensity of the phonons on the left side of the image has been photographically enhanced to accentuate the scattered phonons. (c) Phonon intensity vs angle for the line marked in image (b). The ledge ratio R is the ratio of the scattered to total phonon intensities at the slot.